Silver Nanodisks: Optical Properties Study Using the Discrete Dipole Approximation Method

A. Brioude and M. P. Pileni*

Laboratoire LM2N, Université P. et M. Curie (Paris VI), BP 52, 4 Place Jussieu, F-75231 Paris Cedex 05, France

Received: September 16, 2005; In Final Form: October 13, 2005

The simulated optical properties of silver nanodisks are presented. The extinction, absorption, and scattering efficiencies are calculated using the discrete dipole approximation. The influence of the nanodisk size, truncature (snip), aspect ratio, and environment on the plasmon resonance bands is investigated. In particular, the dipolar and multipolar resonance peak positions have been related to the specific features of the nanodisk geometry. An interpretation of the origins of each multipolar mode is proposed for the first time taking into account this geometry.

1. Introduction

Currently, there is much interest in the optical properties of noble metal nanoparticles. Indeed, these nanoparticles can be used as functional materials in different applications such as near scanning optical microscopy (NSOM),[1−7] surface enhanced spectroscopy,[8−18] chemical and biological sensors,[19−23] optical devices,[24−27] and energy transport.[28−30] This is due, in part, to the strong absorption band exhibited in nanoparticle spectra in comparison to that of bulk. This absorption band results from the interference of the incident photon frequency and the collective oscillation of conduction electrons which is known as localized surface plasmon resonance. This resonance frequency is highly dependent upon the size, shape, dielectric properties, and local environment of the nanoparticles.[31] Understanding those factors that control the absorption response of the nanoparticles with small characteristic dimensions is crucial for the interpretation of experimentally obtained spectra. Recently, it has been possible to produce size- and shape-selected particles by different methods such as nanosphere lithography,[12,32−36] electron-beam lithography,[37,38] and colloid chemistry as reverse micelles.[39−42] This new generation of experimental studies provides important challenges to electrodynamic theory and in particular to numerical simulation efforts.

In this paper, we give a qualitative discussion of the factors that govern plasmon resonance for silver nanodisk by using the discrete dipole approximation (DDA) method.[34,35,43−51] Our applications include studies of the particle size and shape dependence of extinction spectra, the treatment of the local environment, and the influence of the nanodisk fine structure (angles and aspect ratio).

2. Discrete Dipole Approximation (DDA) Method

In the past few years, several numerical methods were developed to determine the optical properties of nonspherical particles, such as the multiple multipole method (MMP),[52,53] the finite difference time domain (FDTD) method,[54−56] and the discrete dipole approximation (DDA).[34,35,43−51] The MMP method was developed for systems with homogeneous, isotropic, and linear material media and is a numerical technique for performing electrodynamic field calculations. The MMP method divides the particle into domains with shapes that allow for series expansion solutions of Maxwell's equations. The coefficients in these expansions are then determined by matching boundary conditions at the domains' interface using the least-squares method so that the resulting solution is exact within each domain but approximate at the boundaries. FDTD methods solve Maxwell's equations as a function of time (rather than at a fixed frequency as with the other methods) using a 3D Cartesian grid for expressing the spatial derivatives. There is also a finite-element version of the same theory.

The DDA is a numerical method first introduced by Purcell and Pennypacker[46] in which the object studied is represented as a cubic lattice of N polarizable point dipoles localized at r_i, $i = 1, 2, ..., N$, each one characterized by a polarizability α_i. There is no restriction on the localization of cubic lattice sites so that the DDA represents a particle of arbitrary shape and composition. The object is excited by a monochromatic incident plane wave $\boldsymbol{E}_{\mathrm{inc}}(r,t) = \boldsymbol{E}_0\, \mathrm{e}^{ik\cdot r - iwt}$, where r, t, w, $k = w/c = 2\pi/\lambda$, c, and λ are the position vector, the time, the angular frequency, the wavevector, the speed of light, and the wavelength of the incident light, respectively. Each dipole of the system is subjected to an electric field consisting of two main contributions: the incident radiation field $\mathbf{E}_{\mathrm{inc},i}$ and the field radiated by all other induced dipoles $\mathbf{E}_{\mathrm{dip},i}$. The local field at each dipole is then given by

$$\mathbf{E}_{i,\mathrm{loc}} = \mathbf{E}_{\mathrm{inc},i} + \mathbf{E}_{\mathrm{dip},i} = \mathbf{E}_0 e^{i\mathbf{k}\cdot\mathbf{r}_i} - \sum_{i\neq j} \mathbf{A}_{ij}\cdot\mathbf{P}_j \qquad (1)$$

P_i is the dipole moment of the ith element and A_{ij} with $i \neq j$ is an interaction matrix with $3N \times 3N$ matrixes as elements described by eq 2.

$$\mathbf{A}_{ij}\cdot\mathbf{P}_j = \frac{e^{ikr_{ij}}}{r_{ij}^{\,3}}\left\{k^2\mathbf{r}_{ij}\times(\mathbf{r}_{ij}\times\mathbf{P}_j) + \frac{(1-ikr_{ij})}{r_{ij}^{\,2}}[r_{ij}^{\,2}\mathbf{P}_j - 3\mathbf{r}_{ij}(\mathbf{r}_{ij}\cdot\mathbf{P}_j)]\right\} \qquad (2)$$

* To whom correspondence should be addressed. E-mail: pileni@sri.jussieu.fr.

10.1021/jp055265k CCC: $30.25
Published on Web 11/19/2005

The 3*N*-coupled complex linear equations given by eq 3 are solved, and each dipole moment $\mathbf{P}_i$ is determined.

$$\mathbf{P}_i = \alpha_i \cdot \mathbf{E}_{i,\mathrm{loc}} \tag{3}$$

The absorption cross sections for a defined target in terms of dipole moments can be derived

$$C_{\mathrm{abs}} = \frac{4\pi k}{|\mathbf{E}_0|^2} \sum_{i=1}^{N} \left\{ \mathrm{Im}[\mathbf{P}_i \cdot (\alpha_i^{-1}) * \mathbf{P}_i^*] - \frac{2}{3} k^3 \left| \mathbf{P}_i \right|^2 \right\} \tag{4}$$

where asterisk means the complex conjugate. We defined the absorption efficiencies as $Q_{\mathrm{abs}} = C_{\mathrm{abs}}/A$ where $A = \pi a_{\mathrm{eff}}^2$, and a_{eff} is defined through the concept of an effective volume equal to $4\pi a_{\mathrm{eff}}^3/3$.

In all the calculations presented here, we consider silver nanoparticles described by the dielectric function ϵ_i measured by Palik.[57]

The surrounding media dielectric constant enters into the calculation through a factor ϵ_0 which is contained in the polarizability α_i. The explicit formula for α_i was developed by Draine and Goodman.[19] To match the experimental conditions of silver nanodisk synthesis previously published,[39−42] the dielectric constant ϵ_0 used in the calculations is 1.94, which corresponds to the value for isooctane, in which the nanodisks are synthesized. Compared to simulations obtained in a vacuum condition, and reported, in general, in other theoretical papers,[2,11] a significant nonlinear red shift of plasmon resonances is observed.

To solve the complex linear equations in the DDA, the code adapted by Draine and Flatau[48] is used. In actual practice, there are significant advantages associated with summing over the dipole fields in eq 1 using the fast Fourier transform method.[47] By substituting eqs 1 and 2 in eq 3, we obtain a relation of the form $\boldsymbol{A'} \cdot \boldsymbol{P} = \boldsymbol{E}$ that we can solve with the complex conjugate gradient techniques. $\boldsymbol{A'}$ is a $3N \times 3N$ matrix built from $\boldsymbol{A}$, and for a system with a total of N elements, $\boldsymbol{E}$ and $\boldsymbol{P}$ are 3*N*-dimensional vectors. One of the advantages of this technique is that it allows a certain arbitrariness in the construction of the array of dipole points that represent the studied target of a given geometry. For example, the geometry of the grid where dipoles have to be located is usually chosen to be cubic but it is not uniquely determined. Obviously, the gridding associated with the DDA calculation creates distortion of the rod surfaces, but except for the layer closest to the surface, the fields are smooth and well converged. In a recent publication,[51] the question of the number of dipoles needed to mimic the continuum macroscopic particle (to approach a homogeneous particle) with an array of discrete dipoles is addressed. The answer is not straightforward, because the convergence of physical quantities is related to this number. Typically, cross sections calculated with the DDA are accurate to a few percent if $N \geq 10^4$ dipoles are used. To avoid problems with the accuracy of the simulations, a very large number of dipoles (at least 40 000) have been used in the calculations. As presented previously, we have a matrix of $(3N)^2$ complex elements that require a large amount of computational effort.

3. Results and Discussion

Face cubic center silver nanodisks,[39−42] with well-defined atomically flat surfaces and differing sizes, are produced. As expected, the optical properties vary with size, geometry, and the surrounding medium. In the following we describe the influence of the various parameters involved on the optical properties. The geometry of the nanodisk, represented in Figure 1, is obtained from a regular tetrahedron cut at the top to adjust the aspect ratio. A truncature, referred to as "snip", is introduced by removing the three other remaining angles. Hence, the nanodisk is mainly defined by three parameters: size, aspect ratio, and snip. Each parameter is determined independently from the others. In all the simulations presented in this paper, we study the influence of one parameter without changing the others. In fact, in many theoretical papers,[51,58] all the geometrical parameters are included in the same parameter a_{eff}. In this case, the modification of the a_{eff} value introduces necessarily a change both in the size and in the shape. The characteristics of the different parameters used are as follows:

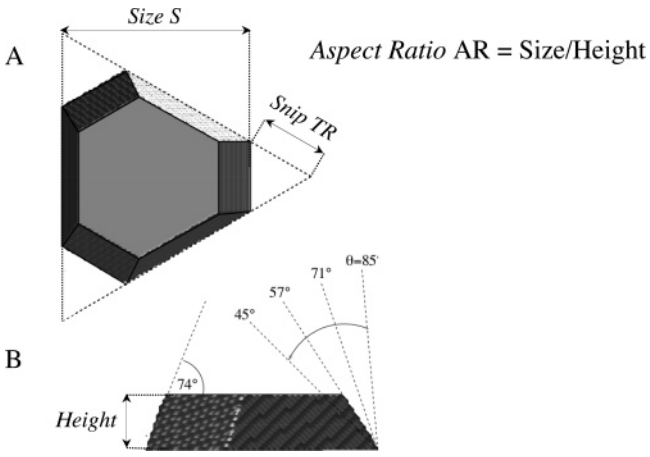

Figure 1. Schematic representation of the nanodisk geometry simulated with the three parameters size (*S*), snip (TR), and aspect ratio (AR): (A) top view; (B) side view.

(i) The nanodisk size *S* is defined as the maximum length of the nanodisk base.

(ii) The aspect ratio, AR, is defined as the ratio of the length of the major to the minor axis.

(iii) The snip, TR, corresponds to the part removed from the tip of the truncated tetrahedron previously obtained. For TR = 0 the object is close to a regular tetrahedron just cut at the top to adjust the aspect ratio.

Concerning the optical properties, several resonance modes can be taken into account in the absorption spectra: (i) dipolar in-plane resonance[42,58,59] (Figure 2A), the most studied resonance and located in the wavelength range between 600 and 1000 nm; (ii) dipolar out-of-plane[42,58,59] resonance (Figure 2B) located around 400−600 nm; (iii) quadrupolar in-plane[42,58,59] resonance (Figure 2C) located around 400−600 nm; (iv) quadrupolar out-of-plane resonance[42,58,59] (Figure 2D) located around 340 nm.

For all these resonances, the position and the intensity vary as a function of the nanodisk geometry and size.

3.1. Influence of the Size of Nanodisks on the Resonance Modes. This influence has been studied for fixed aspect ratio (AR = 4) and two different snips (TR = 0.1 and TR = 0.33).

The increase in the nanodisk size from 20 to 148 nm induces a red shift of the dipolar in-plane resonance mode. This is observed for TR = 0.1 (Figure 3A) and TR = 0.33 (Figure 3B).

The dipolar out-of-plane and quadrupolar in-plane resonance modes can be identified for TR = 0.1 with maxima at 465 and 540 nm, respectively. Conversely on increase of the snip to TR = 0.33 these two modes are not well defined. This is mainly due to the fact that the nanodisk shape is close to a tetrahedron for TR = 0.1 but close to a spherical nanoplate for TR = 0.33.

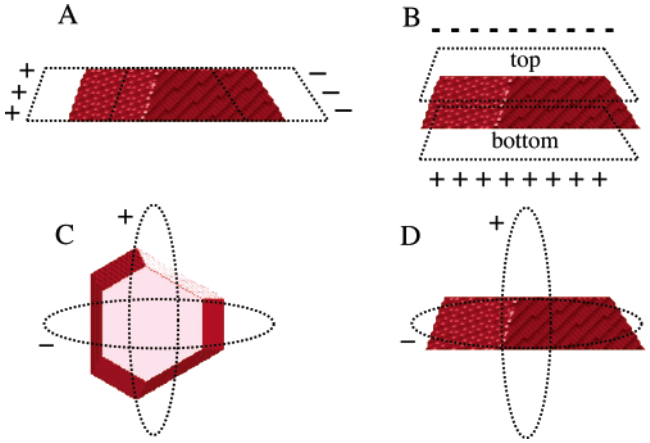

Figure 2. Schematic representation of the resonance plasmon modes involved in the nanodisks. The dipolar in-plane mode and the dipolar out-of-plane mode are represented on (A) and (B), respectively. The corresponding quadrupolar modes are represented on (C) and (D), respectively.

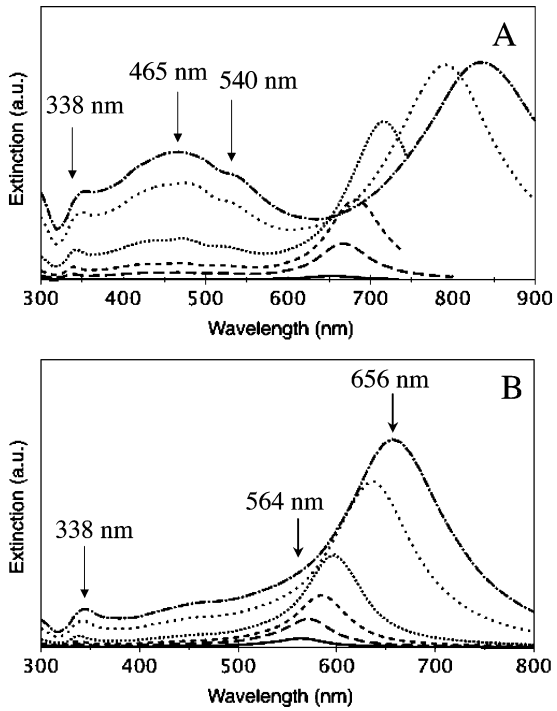

Figure 3. (A) Simulated extinction spectra of nanodisks with parameters AR = 4 and TR = 0.1 for different sizes of S: 20 nm (solid line), 44 nm (— — —), 60 nm (- - -), 86 nm (···), 128 nm (· · ·), 148 nm (- · -). **(**B) Simulated extinction spectra of nanodisks with parameters AR = 4 and TR = 0.33 for different sizes of *S*: 20 nm (—); 44 nm (— — —); 60 nm (- - -); 86 nm (···); 128 nm (· · ·); 148 nm (- · -).

The number of resonance modes in this last case is lower than that expected for a pure tetrahedron. Because of the increase of matter, the extinction coefficient of all the resonances increases with the nanodisk size.

As for the dipolar out-of-plane resonance centered at 465 nm, the in-plane quadrupolar resonance maximum centered at 540 nm linearly increases with increasing the nanodisk size (Insert Figure 4A). The quadrupolar out-of-plane mode is found at around 338 nm and does not change with the nanodisk size.

Whatever the TR value used (TR = 0.1 and TR = 0.33), the maximum wavelength of the in-plane dipolar resonance mode

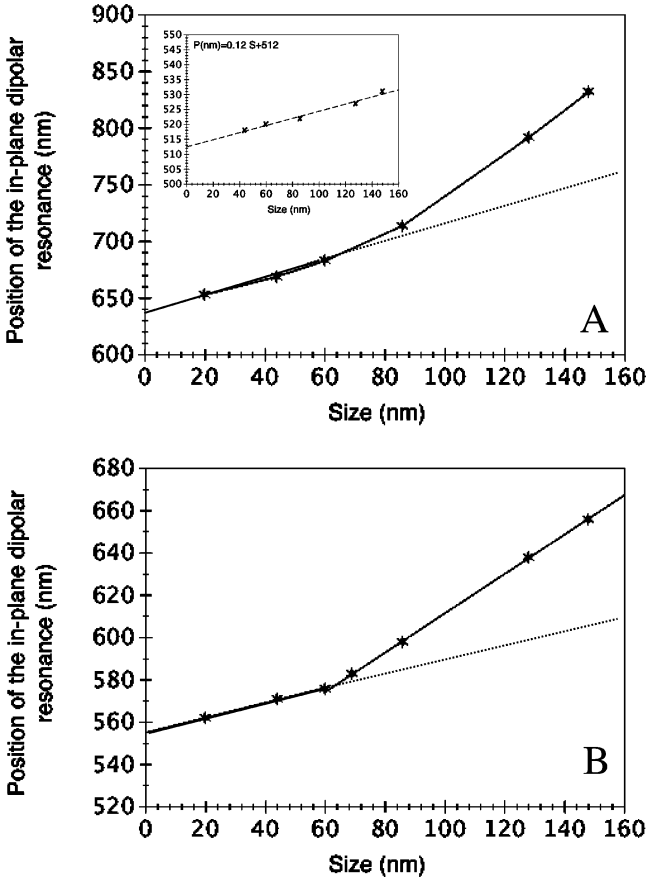

Figure 4. (A) Wavelength position of the in-plane dipolar plasmon resonance as a function of the size of nanodisks with parameters AR = 4 and TR = 0.1. **(**B) Wavelength position of the in-plane dipolar plasmon resonance as a function of the size of nanodisks with parameters AR = 4 and TR = 0.33.

versus the size follows two linear regimes (Figure 4). The intersection point of these two slopes is obtained for a nanodisk with a size of around 60 nm. This value is close to the mean free path of electrons in the bulk (52 nm). Hence, above 60 nm, quadrupolar resonances are expected to appear involving an additional shift in the in-plane dipolar position. Assuming a linear variation of the maximum dipolar in-plane resonance with the particle size, the difference between the two slopes can be explained by the contribution of the quadrupolar in-plane resonance mode that becomes more important and red shifted when the size increases.

3.2. Change of the Resonance Modes with Truncature (snip) for Two Various Nanodisk Sizes. The change in resonance modes with snip are studied for two different nanodisk sizes (105 and 44 nm) keeping the same aspect ratio (AR = 4). In both cases the absorption spectra drastically change for nanodisks with 105 nm (Figure 5) and 44 nm (Figure 6) average size. A blue shift in the in-plane dipolar resonance with increasing snip from TR = 0 to TR = 0.33 is observed for the two sizes. Figure 7 plots the maximum wavelength position of the in-plane resonance mode versus the snip TR. It shows a linear dependence of the wavelength of this mode with TR for nanodisks of 105 nm (square) and 44 nm (circle). To study carefully the influence of the snip from 0 to 0.33 on the quadrupolar (340 nm) and dipolar (426 nm) out-of-plane and quadrupolar in-plane (477 nm) modes, an enhancement of the wavelength region from 315 to 560 nm presented in Figures 5 and 6 is shown in parts A and B of Figure 8, respectively. In both cases (105 and 44 nm), a red shift of the out-of-plane

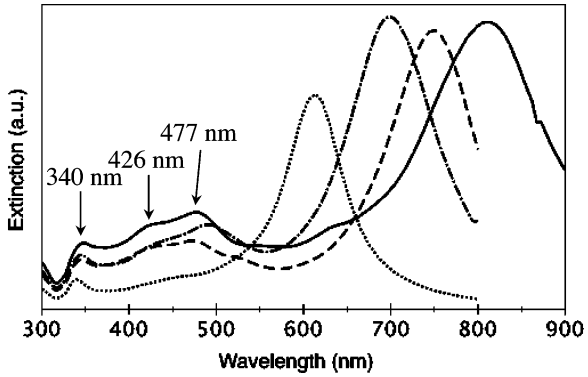

Figure 5. Simulated extinction spectra of nanodisks with parameters $S = 105$ nm and AR = 4 for different snips: TR = 0 (—); 0.1 (- - -); 0.2 (· − ·); 0.33 (···).

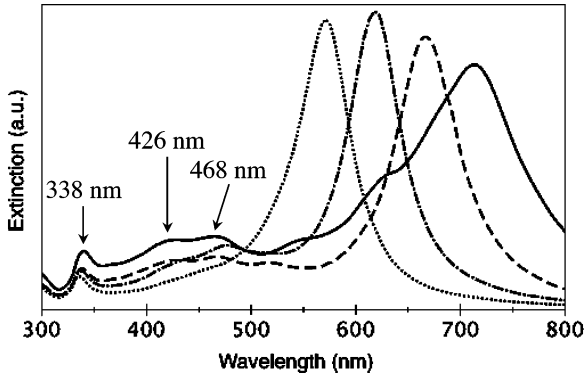

Figure 6. Simulated extinction spectra of nanodisks with parameters $S = 44$ nm and AR = 4 for different snips: TR = 0 (—); 0.1(- - -); 0.2(· − ·); 0.33 (···).

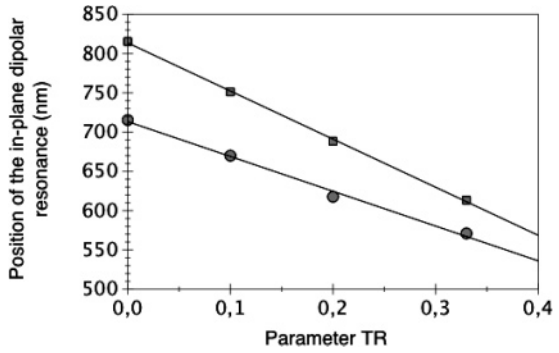

Figure 7. The wavelength position of the in-plane dipolar resonance of nanodisks with AR = 4 as a function of the snip are represented for $S = 44$ nm (circles) and 105 nm (squares). The fit is plotted as a solid line.

quadrupolar resonance with decreasing TR is observed. This is surprising since the modification of the snip should only lead to some changes in the in-plane resonance (Figure 2A). The two other modes do not evolve regularly, and strange behavior for TR = 0.25 is observed. In conclusion, the influence of the snip on the plasmon bands positions and intensities is not well understood for multipolar resonance.

3.3. Influence of the Aspect Ratio on the Dipolar In-Plane Mode. Let us consider nanodisks of the same size ($S = 105$ nm) and snip (TR = 0.33) but differing by their aspect ratio ($1.25 < AR < 10$). Figure 9 shows a red shift of the in-plane dipolar resonance mode with increasing aspect ratio for 105 nm nanodisk. This agrees with previous experimental and theoretical studies of elongated nanoparticles.[59−63] Moreover this

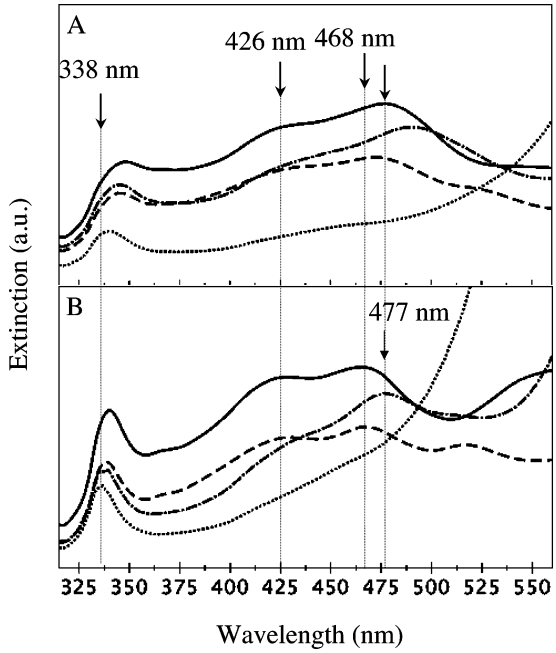

Figure 8. (A) Enlargement of Figure 5 in the range 325−550 nm. **(**B) Enlargement of Figure 6 in the range 325−550 nm.

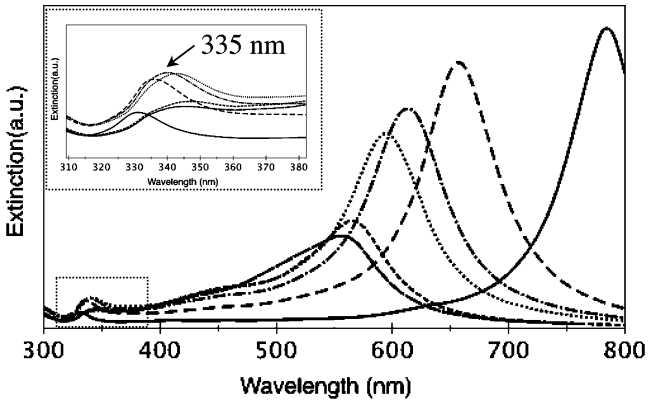

Figure 9. Simulated extinction spectra of nanodisks with parameters $S = 105$ nm and TR = 0.33 for different aspect ratios: AR = 1.25 (− −); 2.4 (- - -); 3.33 (···), 4 (− · −); 5 (- - -); 10 (—). Inset: an enlargement of the extinction spectra in the range 300−380 nm.

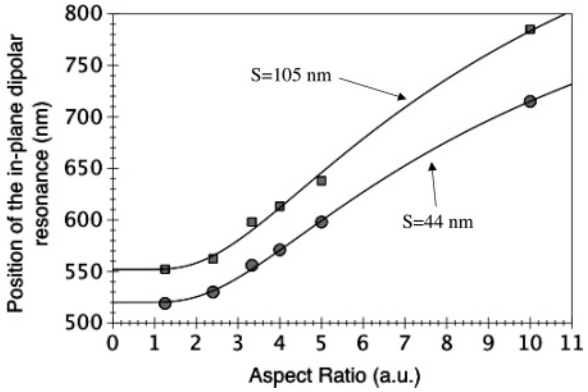

Figure 10. The wavelength position of the in-plane dipolar resonance of nanodisks with TR = 0.25 as a function of the aspect ratio are represented for $S = 44$ nm (circles) and 105 nm (squares). The fit is plotted as a solid line.

shift is observed for two sizes, 44 and 105 nm (Figure 10). In fact the variation of the in-plane dipolar resonance mode with

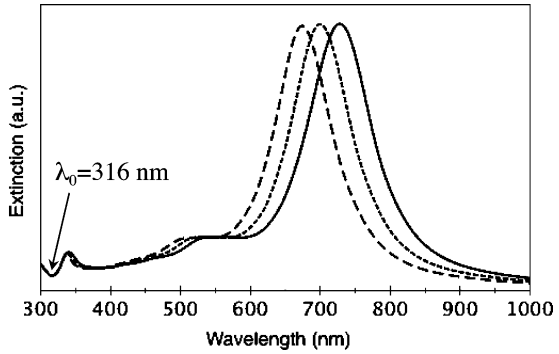

Figure 11. Simulated extinction spectra of 50 nm nanodisks with parameters AR = 4 and TR = 0.33 for three different refractive indexes of the surrounding media: $n = 1.33$ (− − −); 1.39 (- - -); 1.45 (—).

the aspect ratio is specific of the particular geometry to the nanodisk and is given by

$$\lambda(\text{nm}) = a \exp(-9/AR) + \lambda_{\text{min}}$$

where λ_{min} is the blue-shift minimum value for the dipolar in-plane resonance position fixed at 552 nm. The parameter a depends on the nanodisk size and, for TR = 0.33 and for S = 105 nm, is equal to 568.

It should be noted that for other shapes such as nanorods, this variaton is linear.[63]

The insert in Figure 9 shows a blue shift of the quadrupolar out-of-plane resonance mode with increasing aspect ratio. This is explained by the fact that whatever the order of the resonance, on increasing the aspect ratio, the out-of-plane and in-plane modes positions evolve differently. For high aspect ratio, the length of the nanodisk becomes much greater than the height leading to opposite behavior of in-plane and out-of-plane mode. As a consequence, for a low AR, out-of-plane and in-plane resonance modes are comparable and, thus, have close wavelength positions.

3.4. Influence of the Nanodisk Environment on the Resonance Modes. The refractive index of the medium surrounding the nanoparticles is one of the key parameters in determining the position of the resonance bands on the extinction spectra.[64,65] As a consequence, it is well-known that by increasing the refractive index of the solvent, a red shift of all the resonance bands is observed.[58] In many theoretical studies,[51−58] this refractive index is taken at 1, corresponding to that of a vacuum. Those theoretical works bring information concerning the blue-shift limit of resonance bands, since the value of this refractive index cannot be inferior. However, if we consider several resonance plasmon bands in the same absorption spectrum, no previous studies have been done to determine how this shift behaves for all those bands if the refractive index of the solvent is changed. The calculated extinction spectra of a 50 nm silver nanodisk with an aspect ratio of 4 and a snip of 0.33 is shown in Figure 11. Three simulations with various surrounding media such as water, isooctane, and SiO_2 with refractive indexes of 1.33, 1.39, and 1.45, respectively, are reported. It is assumed that the surrounding media does not alter the surface of particles leading to new surface states thereby modifying the position of the resonance bands or their widths.

Whatever the theory used, the only common point of all the spectra calculated in Figure 2 is the position centered at λ_0 = 316 nm. This minimum corresponds to the wavelength at which the dielectric function of silver, both real and imaginary parts, almost vanishes. Therefore, this feature is inherent to the material properties and is independent of the particle geometry and the surrounding medium. Taking into account the wavelength position of a resonance peak λ_1 for a particle embedded in a medium of refractive index n_1, the phenomenological equation which determines the new position of this resonance at λ_2 for this particle in the new media of refractive index n_2 is

$$\lambda_2 = \lambda_1 + (\lambda_1 - \lambda_0)(n_2 - n_1) \qquad (5)$$

TABLE 1

	dipolar in-plane position (nm)		quadrupolar out-of-plane position (nm)	
refractive index	DDA calculation	calcd value with eq 5	DDA calculation	calcd value with eq 5
$n = 1.33$	675.2	675.2	336.8	336.8
$n = 1.39$	699.0	696.8	338.1	338.1
$n = 1.45$	725.0	722.0	340.2	339.4

Table 1 summarizes the wavelength position of the two noticeable resonances and the corresponding calculated values extracted from eq 5. A good agreement between the real wavelength positions of each resonance and the calculated values should allow us to consider each theoretical result obtained in a vacuum ($n = 1$) for comparisons with experimental data for particles in different media. This equation is valid for usual solvent media and of course not for absorbing one where charge transfer should be taken into account in the plasmon bands shift.

3.5. Evolution of the Relative Contribution of Absorption, Extinction, and Scattering Spectra of Different Size Nanodisks. The relative contributions of the absorption (dashed), extinction (straight), and scattered (dotted) spectra of nanodisks of different size are presented in Figure 12. To make a suitable comparison with previous works on particles with simple shapes,[51] for each S size, the corresponding effective diameter ($2a_{\text{eff}}$) is defined by a sphere having an equal volume to the nanodisk considered. For size S = 20, 44, 86, and 128 nm, the corresponding effective diameters are 9.5, 20.5, 40.4, and 60 nm, respectively. For small particles of less than 20 nm, the light absorption process dominates the extinction spectrum (Figure 12A), whereas for large nanoparticles (>50 nm), the light-scattering process becomes important (Figure 12D) and is predominant for larger particles (>100 nm). Here, since the nanodisk geometry is particular, it is necessary to keep in mind that the real size is represented by the parameter S, even though the concept of an effective volume is very useful for the calculations.

3.6. Influence of the Crystallographic Angle on the Optical Properties of Nanodisks. The angles between planes in the nanodisk (Figure 1B) are determined by crystallographic considerations. However, consider a structural deformation by modifying the 57° angle usually fixed by the structure from 45° to 85° keeping same parameters as S (50 nm), AR (4), and TR (0.33). Figure 13 shows no change in the quadrupolar out-of-plane mode (338 nm) and a very small variation of the in-plane dipolar resonance mode (around 700 nm). The slight shift in the wavelength position of the dipolar in-plane mode is not significant, and the quantity of matter increases from 45° to 85° involving an increase in the resonance peak intensity. Conversely, the dipolar out-of-plane (506 nm)[42,58,63] and quadripolar in-plane (573 nm)[42,58,63] modes markedly differ with the angle. At a large angle (85°) the dipolar out-of-plane mode is relatively intense whereas the quadrupolar in-plane mode is negligible. The decrease in the angle from 85° to 45° induces a red shift of the dipolar out-of-plane resonance mode. The increase in the angle leads to an increase in the area of the surface plane on the top of the particle. Thus, the resonance

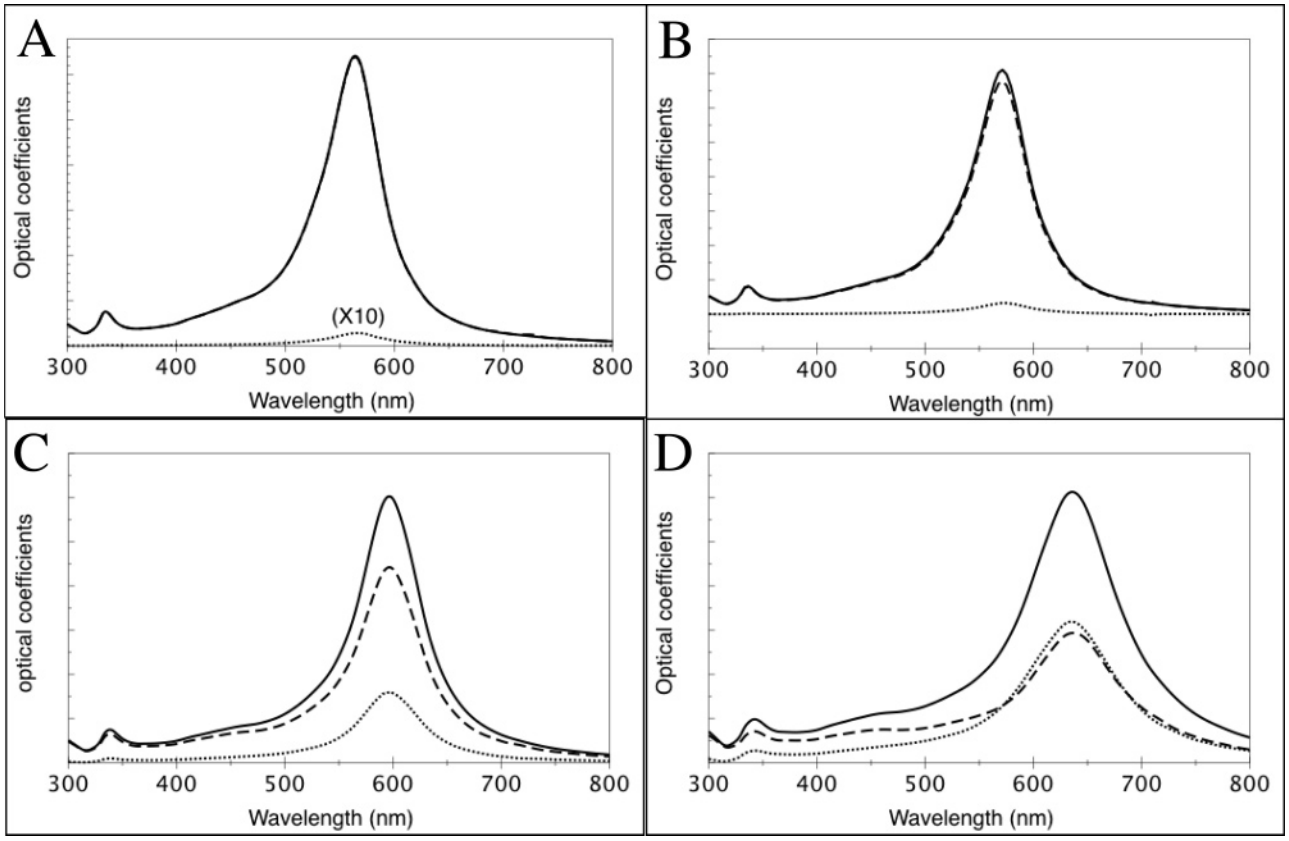

Figure 12. Simulated optical coefficient of nanodisks with parameters AR = 4, TR = 0.33, and S = 20 nm (A), 44 nm (B), 86 nm (C), and 128 nm (D): extinction (—); absorption (− − −); scattering (···).

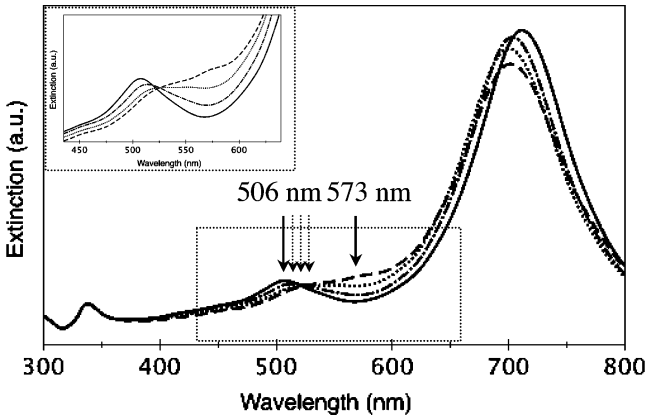

Figure 13. Simulated extinction spectra of 50 nm nanodisks with parameters AR = 4 and TR = 0.33 for different angles: 45° (− − −); 57° (− · −); 71° (···); 85° (—) between nanodisk planes. A description of these angles is given in Figure 1B.

mode intensity is increased but, as the geometry of this surface plane is modified, the position of this resonance also changes. Concerning the other resonance at 573 nm, it seems difficult to deduce significant behavior. In fact, this resonance only appears as a shoulder for an angle of 45° and vanishes for an angle of 85°. The intensity of this peak is too small for a quantitative interpretation.

4. Conclusion

The DDA simulation method is used to determine the evolution of the optical properties of silver nanodisks with various parameters such as size, aspect ratio, snip, and environment. The in-plane dipolar resonance is red shifted with increasing nanodisk size and decreasing snip and shows exponential decay with increasing aspect ratio. A very small variation in the intensity is observed on changing the crystallographic angle of the nanodisk. The out-of-plane quadrupolar resonance remains unchanged on increasing the nanodisk size and is red shifted on increasing the snip and decreasing the aspect ratio. The out-of-plane dipolar and in-plane quadrupolar resonances are red shifted on increasing the snip. In addition, they both markedly differ with the nanodisk crystallographic angle. A phenomenological equation has been proposed to determine the position of all the resonances whatever the media considered.

Acknowledgment. The authors thank Dr. Dinah Parker for fruitful discussions on the writing of this paper.

References and Notes

(1) Knoll, B.; Kellmann, F. *Nature* **1999**, *399*, 134−137.
(2) Sanchez, E. J.; Novotny, L.; Xie, X. S. *Phys. Rev. Lett.* **1999**, *82*, 4014−4017.
(3) Novotny, L.; Bian, R. X.; Xie, X. S. *Phys. Rev. Lett.* **1997**, *79*, 645−648.
(4) Hamann, H. F.; Gallagher, A.; Nesbitt, D. J. *Appl. Phys. Lett.* **1998**, *73*, 1469−1471.
(5) Pufall, M. R.; Berger, A.; Schultz, S. *J. Appl. Phys.* **1997**, *81*, 5689−5691.
(6) Silva, T. J.; Schultz, S. *Rev. Sci. Instrum.* **1996**, *67*, 715.
(7) Stockle, R. M.; Suh, Y. D.; Deckert, V.; Zenobi, R. *Chem. Phys. Lett.* **2000**, *318*, 131.
(8) Metiu, H. *Prog. Surf. Sci.* **1984**, *17*, 153.
(9) Moskovits, M. *Rev. Mod. Phys.* **1985**, *57*, 783.
(10) Jensen, T. R.; Van Duyne, R. P.; Johnson, S. A.; Maroni, V. A. *Appl. Spectrosc.* **2000**, *54*, 371−377.
(11) Yang, W. H.; Hulteen, J. C.; Schatz, G. C.; Van Duyne, R. P. *J. Chem. Phys.* **1996**, *104*, 4313−4323.
(12) Van Duyne, R. P.; Hulteen, J. C.; Treichel, D. A. *J. Chem. Phys.* **1993**, *99*, 2101−2115.
(13) Pipino, A. C. R.; Schatz, G. C.; Van Duyne, R. P. *Phys. Rev. B* **1996**, *53*, 4162−4169.

(14) Michaels, A. M.; Nirmal, M.; Brus, L. E. *J. Am. Chem. Soc.* **1999**, *121*, 9932−9939.
(15) Kneipp, K.; Wang, Y.; Kneipp, H.; Perelman, L. T.; Itzkan, I.; Dasari, R. R.; Feld, M. S. *Phys. Rev. Lett.* **1997**, *78*, 1667.
(16) Nie, S.; Emory, S. R. *Science* **1997**, *275*, 1102.
(17) Xu, H.; Aizpurua, J.; Käll, M.; Apell, P. *Phys. Rev. E* **2000**, *62*, 4318.
(18) Emory, S. R.; Nie, S. *J. Phys. Chem. B* **1998**, *102*, 493−497.
(19) Bauer, G.; Pittner, F.; Schalkhammer, T. *Mikrochim. Acta* **1999**, *131*, 107−114.
(20) Storhoff, J. J.; Elghanian, R.; Mucic, R. C.; Mirkin, C. A.; Letsinger, R. L. *J. Am. Chem. Soc.* **1998**, *120*, 1959−1964.
(21) Elghanian, R.; Storhoff, J. J.; Mucic, R. C.; Letsinger, R. L.; Mirkin, C. A. *Science* **1997**, *277*, 1078−1081.
(22) Lyon, L. A.; Musick, M. D.; Natan, M. J. *Anal. Chem.* **1998**, *70*, 5177.
(23) Schultz, S.; Smith, D. R.; Mock, J. J.; Schultz, D. A. *Proc. Natl. Acad. Sci. U.S.A.* **2000**, *97*, 996.
(24) Dirix, Y.; Bastiaansen, C.; Caseri, W.; Smith, P. *Adv. Mater.* **1999**, *11*, 223−227.
(25) Krenn, J. R.; Dereux, A.; Weeber, V.; Bourillot, E.; Lacroute, Y.; Goudonnet. J. P.; Schider, G.; Gotschy, W.; Leitner, A.; Aussenegg, F. R.; Girard, C. *Phys. Rev. Lett.* **1999**, *82*, 2590.
(26) Weeber, J. C.; Dereux, A.; Girard, C.; Krenn, J. R.; Goudonnet, J. P. *Phys. Rev. B* **1999**, *60*, 9061.
(27) Tominaga, J.; Mihalcea, C.; Büchel, D.; Fukuda, H.; Nakano, T.; Atoda, N.; Fuji, H.; Kikukawa, T. *Appl. Phys. Lett.* **2001**, *78*, 2417.
(28) Quinten, M.; Leitner, A.; Krenn, J. R.; Aussenegg, F. R. *Opt. Lett.* **1998**, *23*, 1331−1333.
(29) Ebbesen, T. W.; Lezec, H. J.; Ghaemi, H. F.; Thio, T.; Wolff, P. A. *Nature* **1998**, *391*, 667−669.
(30) Pendry, J. B. *Science* **1999**, *285*, 1687−1688.
(31) Kreibig, U.; Vollmer, M. Optical Properties of Metal Clusters; Springer-Verlag: Heidelberg, Germany, 1995; Vol. 25.
(32) Hulteen, J. C.; Van Duyne, R. P. *J. Vac. Sci. Technol.* **1995**, *A13*, 1553.
(33) Hulteen, J. C.; Treichel, D. A.; Smith, M. T.; Duval, M. L.; Jensen, T. R.; Van Duyne, R. P. *J. Phys. Chem. B* **1999**, 3854−3863.
(34) Jensen, T. R.; Duval, M. L.; Kelly, L.; Lazarides, A.; Schatz, G. C.; Van Duyne, R. P. *J. Phys. Chem. B* **1999**, *103*, 9846−9853.
(35) Jensen, T. R.; Schatz, G. C.; Van Duyne, R. P. *J. Phys. Chem. B* **1999**, *103*, 2394−2401.
(36) Haynes, C. L.; Van Duyne, R. P. *J. Phys. Chem. B* **2001**, *105*, 5599.
(37) Kahl, M.; Voges, E.; Hill, W. *Spectrosc. Eur.* **1998**, *10*, 12.
(38) Krenn, J. R.; Schider, G.; Rechberger, W.; Lamprecht, B.; Leitner, A.; Aussenegg, F. R. *Appl. Phys. Lett.* **2000**, *77*, 3379.
(39) Maillard, M.; Giorgio, S.; Pileni, M. P. *Adv. Mater.* **2002**, *14*, 1084.
(40) Maillard, M.; Giorgio, S.; Pileni, M. P. *J. Phys. Chem. B* **2003**, *107*, 2466.
(41) Germain, V.; Li, J.; Ingert, D.; Wang, Z. L.; Pileni, M. P. *J. Phys. Chem. B* **2003**, *107*, 8717.
(42) Germain, V.; Brioude, A.; Ingert, D.; Pileni, M. P. *J. Chem. Phys.* **2005**, *122*, 1.
(43) Yang, W. H.; Schatz, G. C.; Van Duyne, R. P. *J. Chem. Phys.* **1995**, *103*, 869.
(44) Kelly, K. L.; Lazarides, A. A.; Schatz, G. C. *Comput. Sci. Eng.* **2001**, *3*, 67.
(45) Mishchenko, M. I.; Hovenier, J. W.; Travis, L. D. *Light Scattering by Nonspherical Particles*; Academic Press: San Diego, CA, 2000.
(46) Purcell, E. M.; Pennypacker, C. R. *Astrophys. J.* **1973**, *186*, 705.
(47) Draine, B. T. *Astrophys. J.* **1998**, *333*, 848. Draine, B. T.; Goodman, J. J. *Astrophys. J.* **1993**, *405*, 685. Draine, B. T.; Flatau, P. J. *J. Opt. Am. A* **1994**, *11*, 1491.
(48) Draine, B. T.; Flatau, P. J. Program DDSCAT; University of California at San Diego: San Diego, CA.
(49) Malinsky, M. D.; Kelly, K. L.; Schatz, G. C.; Van Duyne, R. P. *J. Phys. Chem. B* **2001**, *105*, 2342.
(50) Malinsky, M. D.; Kelly, K. L.; Schatz, G. C.; Van Duyne, R. P. *J. Am. Chem. Soc.* **2001**, *123*, 1471.
(51) Sosa, I. O.; Noguez, C.; Barrera, R. G. *J. Phys. Chem. B* **2003**, *107*, 6269−6275.
(52) Novotny, L.; Pohl, D. W.; Hecht, B. *Opt. Lett.* **1995**, *20*, 970−972.
(53) Moreno, E.; Erni, D.; Hafner, C.; Vahldieck, R. *J. Opt. Soc. A* **2002**, *19*, 101.
(54) Taflove, A. *Computational Electrodynamics: The Finite-Difference Time-Domain method*; Artech House: Boston, 1995; p 599.
(55) Kahnert, F. M. *J. Quant. Spectrosc. Radiat. Transfer* **2003**, *79−80*, 775−824.
(56) Futamata, M.; Maruyama, Y.; Ishikawa, M. *J. Phys. Chem. B* **2003**, *107*, 7607−7617.
(57) Lynch, D. W.; Hunter, W. R. In *Handbook of Optical Constants of Solids*; Palik, E. D., Ed.; Academic Press: New York, 1985; pp 350−356.
(58) Kelly, K. L.; Coronado, E.; Zhao, L. L.; Schatz, G. C. *J. Phys. Chem. B* **2003**, *107*, 668−677.
(59) Jin, R.; Cao, Y.; Mirkin, C. A.; Kelly, K. L.; Schatz, G. C.; Zheng, J. G. *Science* **2001**, *294*, 1901.
(60) Mohamed, M. B.; Ismail, K. Z.; Link, S.; El-Sayed, M. A. *J. Phys. Chem. B* **1998**, *102*, 9370−9374.
(61) Perez-Juste, J.; Liz-Marzan, L. M.; Carnie, S.; Chan, D. Y. C.; Mulvaney, P. *Adv. Funct. Mater.* **2004**, *14*, 6.
(62) Link, S.; Burda, C.; Nikoobakht, B.; El-Sayed, M. A. *Chem. Phys. Lett.* **1999**, *315*, 12−18.
(63) Yu, Y. Y.; Chang, S.-S.; Lee, C. L.; Wang, C. R. C. *J. Phys. Chem. B* **1997**, *101*, 6661.
(64) Al-Sayed, A.; Majied, A.-S. *Colloids Surf., A* **2004**, *246*, 61−69.
(65) Charlé, K. P.; Franck, F.; Schulze, W. *Ber. Bunsen-Ges. Phys. Chem.* **1984**, *88*, 350.
(66) Hövel, H.; Fritz, S.; Hilger, A.; Kreibig, U.; Vollmer, M. *Phys. Rev. B* **1993**, *48*, 18178.
(67) Mulvaney, P. *Langmuir* **1996**, *12*, 788.